Scientific Reports

https://doi.org/10.1038/s41598-026-43216-1

Article in Press

Highly sensitive electrochemical detection and quantification of opium derived morphine sulfate using cysteamine loaded MWCNTs@V_2O_5 telluride composite

Received: 24 May 2025

Accepted: 2 March 2026

Published online: 15 March 2026

Cite this article as: Shaheen S., Fatima B., Hussain D. *et al.* Highly sensitive electrochemical detection and quantification of opium derived morphine sulfate using cysteamine loaded MWCNTs@V_2O_5 telluride composite. *Sci Rep* (2026). https://doi.org/10.1038/s41598-026-43216-1

Sana Shaheen, Batool Fatima, Dilshad Hussain, Ayub Alam, Muhammad Ayub & Muhammad Najam-ul-Haq

Highly Sensitive Electrochemical Detection and Quantification of Opium Derived Morphine Sulfate using Cysteamine Loaded MWCNTs@V_2O_5 Telluride Composite

Sana Shaheen[1], Batool Fatima[1]*, Dilshad Hussain[2], Ayub Alam[3], Muhammad Ayub[4], Muhammad Najam-ul-Haq[5]*

[1]: Department of Biochemistry, Bahauddin Zakariya University, Multan, 60800, Pakistan

[2]: HEJ Research Institute of Chemistry, International Center for Chemical and Biological Sciences, University of Karachi, Karachi 75270, Pakistan

[3]: Department of Chemistry, The Islamia University of Bahawalpur, Bahawalnagar Campus, Bahawalnagar, Pakistan.

[4]: Institute of Biochemistry, University of Balochistan, Quetta, Pakistan.

[5]: Institute of Chemical Sciences, Bahauddin Zakariya University, Multan, 60800, Pakistan

*Corresponding Author (s)

Dr. Batool Fatima (batoolfatima@bzu.edu.pk)

Prof. Dr. M. Najam-ul-Haq (najamulhaq@bzu.edu.pk)

Abstract

A novel electrochemical sensor based on multi-walled carbon nanotubes doped with vanadium pentoxide/telluride (MWCNTs@V_2O_5/Te) is developed for the detection and quantification of morphine sulfate in real biological samples. MWCNTs@V_2O_5/Te nanocomposite was functionalized with cysteamine as a linker, to create thiol interaction with the -OH group of the MWCNTs@V_2O_5/Te nanocomposite at one end, and free -NH_2 group interaction with the -OH group on morphine sulfate, on the other end. This modification enhances the conjugation capability of morphine sulfate with the fabricated biosensor, thereby modifying the glassy carbon electrode (MWCNTs@V_2O_5/Te-Cys/GCE). MWCNTs@V_2O_5/Te nanocomposite morphological and structural analysis was carried out via SEM, TEM, EDX, FTIR, and UV-Vis spectroscopy. At varying concentrations and pH levels, the electrochemical sensor response of the modified electrode was investigated using cyclic voltammetry (CV). To validate the findings, differential pulse voltammetry (DPV), electrochemical impedance spectroscopy (EIS), and chronoamperometry were employed to cross-check morphine sulfate detection, yielding excellent results for its determination in real biological samples. The fabricated sensor, as indicated by the calibration curve, exhibits a wide linear range of 10-60 µM and a limit of detection (LOD) of approximately 0.01 µM for DPV. These parameters revealed that this novel sensor is highly stable, sensitive, and reproducible for detecting morphine sulfate. Furthermore, this developed sensing platform shows promise in clinical diagnostics, narcotics detection, and forensic analysis.

Keywords: Electrochemical sensing, Morphine sulfate, Multi-walled carbon nanotubes, Clinical diagnosis, Real biological sample.

1. Introduction

Papaver Somniferum (Opium poppy) is a species from the Papaveraceae family, naturalized in Asia and Europe, but native to the eastern Mediterranean. The term "poppy" means "sleep" [1, 2]. It possesses exceptional antioxidant, analgesic, and antimicrobial properties. Grounded the raw opium into powder form and then converted it into derivatives like codeine, heroin, and morphine after many treatments. Among 20 or more alkaloids of opium, the most important is morphine, which is primarily responsible for opium narcotics [3]. The 10-20% content in opium is based on alkaloids, and only six alkaloids are in significant concentration in opium: morphine, noscapine, codeine, thebaine, nicotine, and benzylisoquinoline papaverine, while other alkaloids are in traces [4, 5]. Morphine is derived from the Greek word "morphos," meaning "God of sleep," and is a natural opium alkaloid isolated in 1806 by Friedrich Serturner and first synthesized in 1952. It is metabolized in the intestinal wall, liver, central nervous system, and kidneys. After oral administration, the plasma half-life of morphine is approximately 2.5-3 hours, while after parenteral administration, its half-life is around 1-1.5 hours [6]. Morphine sulfate ($C_{34}H_{40}N_2O_{10}S$) is one of the most potent analgesic drugs utilized in pain management and active cancer treatment, and provides relief to patients afflicted with chronic pain. The pharmacodynamic effects of morphine are exerted via its agonist action with the μ-opioid receptor, as it acts as the primary target responsible for the respiratory depression and analgesia [7, 8]. Morphine also has a risk for addiction and abuse, which can lead to overdose and eventually death. To minimize the risk of addiction, use the smallest or optimal dose of morphine [9, 10].

Previously reported methods commonly employed for morphine detection i.e., gas chromatography (GC) [11, 12], high-performance liquid chromatography (HPLC) [13, 14], immunoassays, radioimmunoassay (RAI) [15], capillary electrophoresis (CE) [16] as well as surface plasmon resonance (SPR), but face some limitations majorly including long

analysis time, expensive reagents, and equipment [1]. Whereas, electroanalytical methods play a crucial role in the detection and quantification of biologically active substances and environmental contaminants due to their sensitivity and rapid response. These techniques have demonstrated exceptional potential in identifying pharmaceuticals, drugs of abuse, and biomolecules, even in complex matrices such as blood serum and wastewater [17-21]. The electrochemical method offers on-site, real-time analysis and ease of handling. To create selective and sensitive sensors for determining specific analytes, a large number of high-performance electrochemical sensors are being synthesized. Due to their significance, electrochemical sensors have garnered considerable attention in analytical research [22-24].

The transducer in the biosensor is typically a nanomaterial with a large surface area, high electrical conductivity, and compatibility with the analyte molecule. These nanomaterials enhance the performance and conductivity of biosensors, while also providing low detection ranges and increasing their sensitivity [25]. Modern nanomaterials are used to develop innovative, selective electrochemical biosensors [26, 27], which, when combined with surface modification and bioconjugation, enhance the signal-carrying capacity of signal tracers and facilitate electron transfer [25]. Carbon nanotubes (CNTs) immobilized on an electrode facilitate electrochemical sensing through their conductivity, chemical stability, and large surface area, thereby enhancing electron transfer reactions. Multi-walled carbon nanotubes (MWCNTs) with COOH groups on the electrode increase surface area and serve as carriers for immobilizing multiple antibodies. MWCNTs exhibit faster, stronger signal responses due to their high electrical conductivity [21, 26-28]. Transition metal oxides (TMOs) typically enhance the conductivity of the electrochemical sensors developed. For example, vanadium pentoxide (V2O5) coating on MWCNTs enhances electron conductivity, making it a promising candidate for improving electrochemical performance and facilitating interfacial electron transfer [29, 30]. Telluride (Te) is a rare,

attractive material with a conductive crystal structure and high electronic conductivity. During electrochemical oxidation-reduction reactions, Te exhibits a higher density of active sites for electrocatalytic applications, is tolerant, and has a high specific surface area [31, 32].

MWCNTs@V_2O_5/Te nanocomposite functionalized with cysteamine modified GCE was employed for the electrochemical determination of morphine sulphate in synthetic buffer solutions and serum samples via cyclic voltammetry and differential pulse voltammetry. The electrode's electrochemical behavior was examined after each modification step. The outcomes exhibit good linearity and sensitivity.

2. Experimental

2.1 Chemicals and reagents

Multi-walled carbon nanotubes (MWCNTs) having 6-13 nm in diameter and 2.5-20 µm in length with ˃98% purity was purchased from Sigma-Aldrich, sulphuric acid (H_2SO_4, 98%), nitric acid (HNO_3, 65%), distilled water, ethanol (C_2H_5OH, 96%), pH paper strips, vanadium pentoxide (V_2O_5, 98%), hydrogen peroxide (H_2O_2, 30%), telluride powder (98%), hydrazine monohydrate ($N_2H_4.H_2O$, 80%), deionized water (DI water), cysteamine (C_2H_7NS, 95%) and ferric cyanide (C_3FeN_3, 98%), all these chemicals and reagents were purchased from Sigma-Aldrich and these were used in the experiments without any further purification processes. Morphine sulfate ($C_{34}H_{40}N_2O_{10}S$, 95%) was obtained from McKesson Medical-Surgical. All solutions were prepared in distilled and deionized water.

2.2 Functionalization/Oxidation of Multi-Walled Carbon Nanotubes (MWCNTs)

50 mg of MWCNTs were taken in a beaker, and then 8mL of H2SO4:HNO_3 solution (3:1 vol/vol, with an initial concentration of 90%) was added using a 1mL pipette tip to complete the exothermic reaction for 30 min. Once MWCNTs settled to the bottom of the beaker, the

solution was sonicated at 160 W and 60°C for 1 hour. Using a micropipette, 30 mL of distilled water was added dropwise to the MWCNTs-COOH solution, and then the solution was transferred to a centrifuge tube. At room temperature, the MWCNTs-COOH solution was centrifuged at 6000 rpm for 30 min. After centrifugation, the supernatant was removed using 1 mL pipette tips. In the same centrifuge tube, 6 mL of ethanol was added, and the solution was then centrifuged at 6000 rpm for 20 min. Until the supernatant reached neutrality (pH 7), the washing/centrifugation steps were repeated. Afterwards, with the help of 1 mL pipette tips, the supernatant was removed and distilled water (1 mL) was added to disperse and precipitate the functionalized MWCNTs-COOH [33]. Lastly, the MWCNTs-COOH precipitates were dried at 60°C for 2 hours.

2.3 Synthesis of MWCNTs@V_2O_5 Nanorods

For the synthesis of MWCNTs@V_2O_5 nanosheet composites, 1.02 g of the crystalline powder of V_2O_5 was dissolved slowly in 80 mL of hydrogen peroxide solution (30%), and during the reactive process, an exothermic reaction takes place to form a precursor of brown solution, and the reaction is mentioned below [34]:

$$V_2O_5 + 4H_2O_2 \rightarrow 2[VO(O_2)_2]^- + 3H_2O + 2H^+ \quad (1)$$

After 30 minutes, the pretreated aqueous solution of MWCNTs (0.18 g in 10 mL of distilled water) was added to the above red/brown solution, forming a black colloidal suspension. The solution was stirred for 6-8 hours, then aged for approximately 24 hours, after which it gradually transformed into a hydrogel. The resulting MWCNTs@V_2O_5 nanorods were transferred into a Teflon-lined stainless-steel autoclave and heated to 180 ℃ for 3 days. After that, the product was filtered and vacuum-dried at 80 ℃ for 8 hours, yielding MWCNTs@V_2O_5 nanosheets [35].

2.4 Synthesis of MWCNTs@V_2O_5/Te Nanocomposite

MWCNTs@V_2O_5/Te nanocomposite was prepared by the solvent mixing process and filtration. 1.02 g of telluride powder was dispersed in a 100 mL ethanol solution containing approximately 0.18 g of MWCNTs@V_2O_5 nanosheet composites, and then the mixture was ultrasonicated for about 1 h. By adding approximately 3 mL of hydrazine monohydrate (N2H4.H2O), the dispersion was reduced, and the mixture was heated with stirring at 80 ℃ for approximately 1 hour. Filtered the resulting MWCNTs@V_2O_5/Te nanocomposite with deionized water and dried for 24 h at 60 ℃, and the final product was ground into a fine powder, as illustrated in Figure 1. [36].

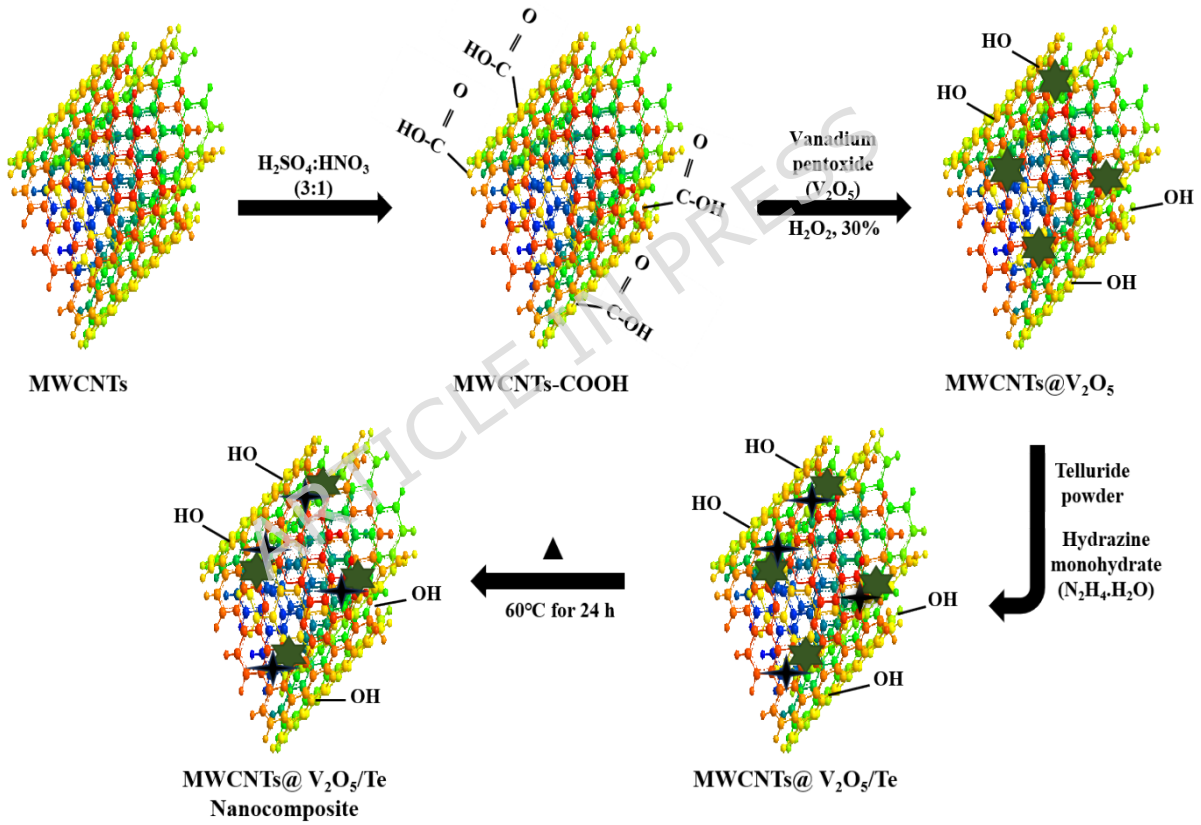

Figure 1. *Synthesis of* MWCNTs@V_2O_5/Te *nanocomposite.*

2.5 MWCNTs@V_2O_5/Te Nanocomposite modified with Cysteamine and Preparation of Working Electrode

Prepare a 0.1 M solution of cysteamine by dissolving 0.6 g in 25 mL of deionized water. The working electrode was prepared by fabricating MWCNTs@V_2O_5/Te nanocomposite on the GCE. Then, that electrode was

dipped in a 0.1 M solution of cysteamine at 37 ℃ and subsequently dried for 3 h [37]. MWCNTs@V_2O_5/Te nanocomposite was functionalized with the linker cysteamine as cysteamine has -SH group which create thioether bond interaction with the -OH group of the MWCNTs@V_2O_5/Te nanocomposite that is illustrated in Figure 2. and at the other end of the linker free -NH_2 group react with the -OH group on morphine sulfate in the presence of the iron as enzyme, employed in form of ferric cyanide.

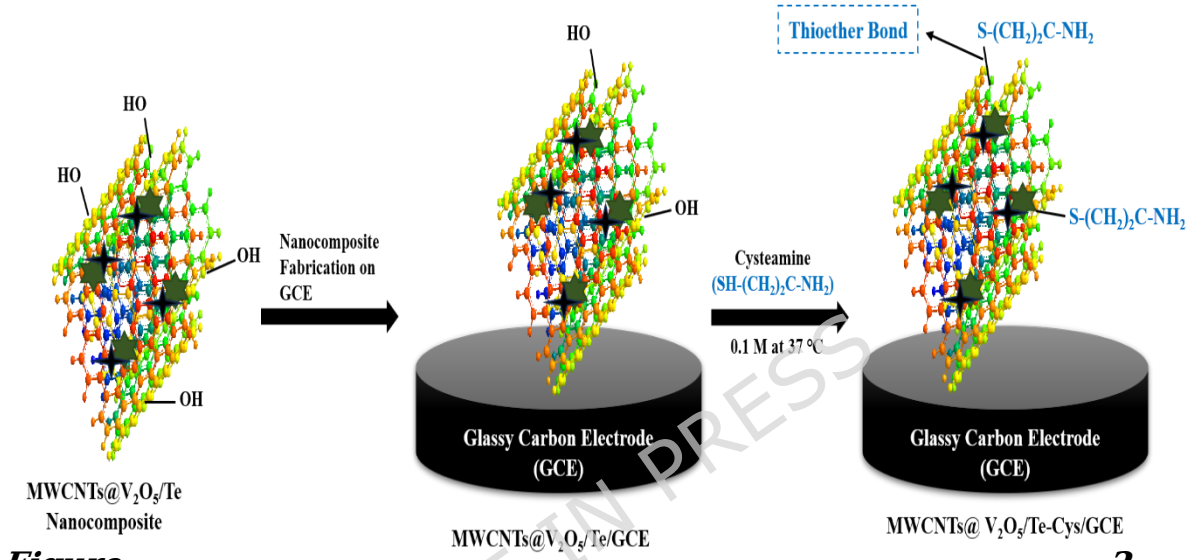

Figure 2.

Synthesis of MWCNTs@V_2O_5/Te-Cys/GCE.

2.6 Electrochemical Sensing of Morphine Sulfate

Alumina powder suspension and polishing cloth were used to polish the electrode and remove contaminants. The electrode was then sonicated in ethanol for 15 minutes. It was washed with ultra-pure or deionized water. The biosensor was fabricated onto an electrode, modified with cysteamine, and then dried for 1 hour at room temperature. Cyclic voltametric measurements were performed at pH 7.4 in 0.1 M phosphate-buffered saline (PBS) buffer (prepared in distilled water) with a scan rate of 30 mV/s. The voltammetric analysis evaluated the biosensor's performance by varying morphine sulfate concentration and pH in PBS buffer.

2.7 Serum Sample Collection and Processing

Rabbits were purchased from a local rabbit farm. Real sample collection and analysis were conducted on rabbits in accordance with the guidelines of the Ethical Committee of Bahauddin Zakariya University, Multan, Pakistan. Blood samples were taken from three male rabbits weighing approximately 3 kg. A 60 µM solution of morphine sulfate was then prepared, from which 3 mL was injected into the rabbits. These rabbits were kept under normal conditions. As a result, morphine sulfate provided relief to the rabbits afflicted with severe and chronic pain. After 2, 4, and 6 hours, blood samples were collected in sample tubes. The blood samples were centrifuged at 4000 rpm for 10 min to obtain serum for morphine sulfate detection. All the animal experiments were performed in accordance with the ARRIVE guidelines.

3. Results and Discussion

3.1 Characterization of MWCNTs@V_2O_5/Te Nanocomposite

Nanocomposite size, structural appearance, and surface morphology are evaluated by scanning electron microscopy (SEM) (Jeol, Kyoto, Japan). In Figures 3(A) and 3(D), SEM images indicate that the MWCNTs@V_2O_5/Te nanocomposite is in the form of nanorods, and during the doping process, the surface morphology of MWCNTs does not change. Histogram in Figure 3(B). shows that MWCNTs@V_2O_5 size distribution is in the range of 12-28 nm with an average diameter of 19nm, while the histogram in Figure 3(E) depicts that MWCNTs@V_2O_5/Te nanocomposite size distribution is in the range of 16-30 nm with an average diameter of 23 nm. The transmission electron microscopy (TEM) image in Figure 3(G) shows the consistent density and internal structure of the MWCNTs@V_2O_5/Te nanocomposite with a higher resolution than the SEM images. Energy-dispersive spectroscopy (EDS) was performed using an EDS system (S3700N, Hitachi, Japan) to qualitatively analyze the prepared material. Figure 3(C) shows that the nanomaterial consists of 30% C, 40.27% V, and 30.73% O. In contrast, Figure 3(F) shows that the nanomaterial consists of 16.90% O and 83.10% Te. The O content of the prepared nanomaterial indicates that it undergoes oxidation during

synthesis. As a result, the EDS graph shows the uniform distribution of C, V, O, and Te in the prepared nanocomposite.

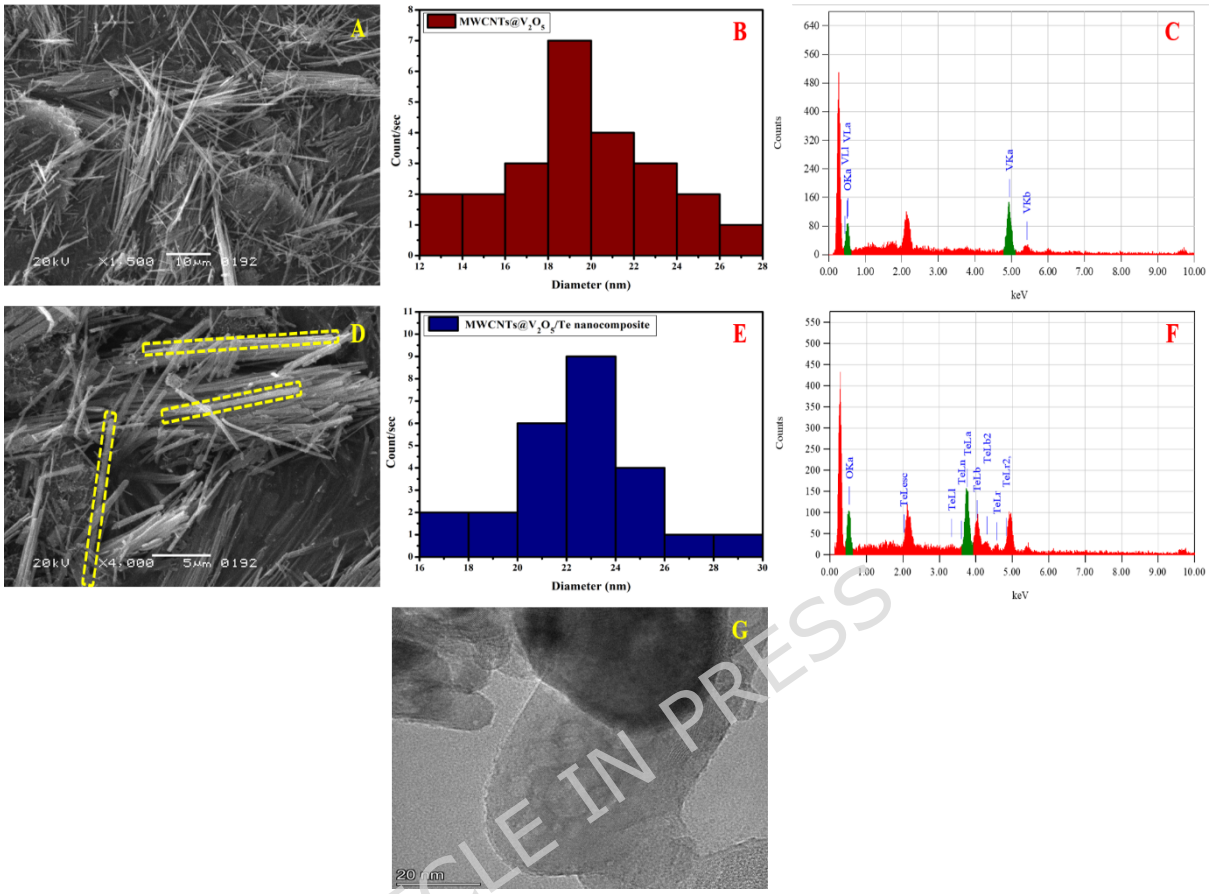

Figure 3. ***(A, D)*** *SEM images of MWCNTs@V_2O_5 and MWCNTs@V_2O_5/Te,* ***(B, E)*** *depict the histograms of particle size distribution of MWCNTs@V_2O_5 and MWCNTs@V_2O_5/Te,* ***(C, F)*** *represent the EDS graph of MWCNTs@V_2O_5 and MWCNTs@V_2O_5/Te,* ***(G)*** *TEM image of MWCNTs@V_2O_5/Te.*

X-ray diffraction (XRD) analysis of synthesized samples was conducted utilizing a Bruker D8 Advance Powder Diffractometer. XRD analysis of MWCNTs-COOH is shown in Figure 4A(a). MWCNTs show a characteristic peak at 25.8°, which is related to the (002) plane. MWCNTs@V_2O_5 composite shows peaks at 21.9°, 33.1°, 35.5°, 41.9°, 47.7°, 58.6°, and 62.1° with hkl planes of (110), (111), (301), (020), (600), (421), and (701) respectively in Figure 4A(b). These patterns align with the known patterns of V_2O_5 (01-0359). Furthermore, MWCNTs@V_2O_5/Te exhibited additional diffraction peaks at 23.4° and

27.9°, 44.5° and 49.9°, which correspond to the hkl values of (100), (101), (003), and (201), respectively, as illustrated in Figure 4A(c). These peaks coincide with the standard pattern of tellurium (36-1452).

Bragg's law determines the d-spacing, or interatomic spacing.

$$d = \frac{n\lambda}{2\sin\theta} \quad (2)$$

The average d-spacing or inter-atomic spacing of MWCNTs, MWCNTs@V_2O_5, and MWCNTs@V_2O_5/Te is 3.46 Å, 2.34 Å, and 2.55 Å, respectively.

The crystallite size is calculated by the Scherrer formula.

$$D = 0.9\lambda/\cos\theta\beta \quad (3)$$

λ indicates the wavelength of X-rays, the angle of the incident radiation is indicated by θ, and β is the peak width at half maximum. The average crystallite size of MWCNTs, MWCNTs@V_2O_5, and MWCNTs@V_2O_5/Te is 4.07 nm, 17.32 nm, and 11.66 nm, respectively.

A Fourier-transform infrared (FTIR) spectrum is obtained for transmittance measurements from 4000 to 500 cm^{-1} using a Bruker INVENIO FTIR Spectrometer in Germany. For the interpretation of functional groups, IR spectra were divided into three regions. As in these regions, peaks in the range of 700-800 cm^{-1} are assigned to the characteristic stretching of the C-O bond, and the peaks that appear in the range of 1550-1750 cm^{-1} are assigned to the C=O groups, which are characteristic of quinone/ketone and carboxylic acid [38]. Figure 4(B) illustrates that in these regions, the peaks at 1718 cm^{-1} are mainly assigned to the stretching of C=O [38, 39], while the peaks at 2600 cm^{-1} to 2700 cm^{-1} show the stretching of the C-H bond in the aliphatic groups, i.e., -CH_2 and -CH_3. The peaks at 3000-3600 cm^{-1} show the stretching of the -O-H bond in carboxyl and hydroxyl groups. In the 2nd and 3rd regions, the peaks at 900-1200 cm^{-1} are assigned to terminal stretching of the oxygen atom in the V=O bond in V_2O_5 [40, 41]. In the 3rd region,

the peak at 900 cm^{-1} corresponds to the O-Te-O group [40]. The peaks of the doped nanocomposite, MWCNTs@V_2O_5/Te, are higher than those of the undoped material.

AQ7100APAC Thermo Fischer Scientific UK Spectrophotometer is used for UV-Vis analysis to study the absorption spectra of MWCNTs-COOH, MWCNTs@V_2O_5, and MWCNTs@V_2O_5/Te nanocomposite. Figure 4(C) illustrates absorption spectra in the range of 230-440 nm. The literature review suggests that MWCNTs-COOH exhibits absorptions in the 240-265 nm range [43, 44]; in our case, the absorption peak is observed at 253 nm. V_2O_5 shows a UV-Vis absorption spectrum in the range of 230-350 nm [41]. V_2O_5 doped on MWCNTs shows a peak at 255 nm, and telluride (Te) shows an absorption peak at 260 nm, thus indicating UV-absorption intensities increase by doping metals on MWCNTs as compared to MWCNTs-COOH. With the help of the following equation, the band gap is calculated as:

$$E = \frac{1240}{\lambda(nm)} eV \quad (4)$$

UV-Vis absorption peaks of MWCNTs@V_2O_5 and MWCNTs@V_2O_5/Te nanocomposite are at 255 nm and 260 nm, and the calculated band gaps are about 4.8 eV and 4.7 eV, respectively, which shows little or no

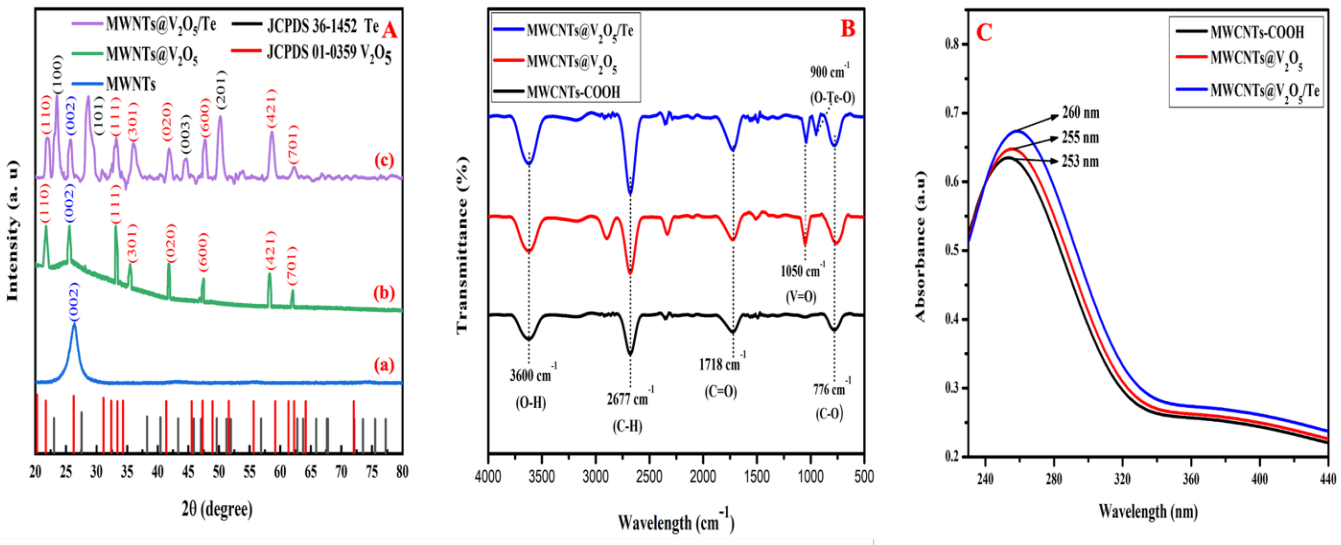

significant change in band gaps.

Figure 4. (A) *XRD patterns,* ***(B)*** *FTIR, and* ***(C)*** *UV-Visible spectra of MWCNTs-COOH, MWCNTs@V_2O_5, and MWCNTs@V_2O_5/Te.*

3.2 Cyclic Voltammetry of MWCNTs@V_2O_5/Te Nanocomposite

Oxidation-reduction processes are typically measured using cyclic voltammetry (CS350M potentiostat/galvanostat with EIS) between morphine sulfate and MWCNTs@V_2O_5/Te [42]. In 0.1 mM $[Fe(CN)_6]^{3-/4-}$ and 0.1 M KCl solutions, a cyclic voltammogram is obtained by immobilizing MWCNTs@V_2O_5/Te onto bare GCE. Figure 5(A) shows that redox peaks are shown by undoped and doped nanocomposites, while there is no peak of oxidation and reduction on bare GCE. At 0.3 V, the oxidation peak takes place. In contrast, the reduction peak is observed at 0.1 V. Figure 5(A) indicates that MWCNTs-COOH exhibits less conductivity, whereas MWCNTs@V_2O_5 and MWCNTs@V_2O_5/Te nanocomposite have higher conductivity. Therefore, by doping V_2O_5 and Te on MWCNTs, an increase in peak current illustrates that the doped nanocomposite has higher conductivity due to an elevation in the number of free electrons compared to the undoped material. The stability of MWCNTs@V_2O_5/Te in 0.1 mM of $[Fe(CN)_6]^{3-/4-}$ and in 0.1 M of KCl solutions is depicted in Figure 5(B). MWCNTs@V_2O_5/Te behavior indicates that it is highly stable and conductive and can be employed for the detection of morphine sulfate.

3.2.1 Electrochemical Surface Area (ECSA) of MWCNTs@V_2O_5/Te

ECSA of MWCNTs@V_2O_5/Te is determined in 0.1 mM of $[Fe(CN)_6]^{3-/4-}$, and 0.1 M of KCl solutions in a 1:1 ratio. Cyclic voltammetric analysis is performed at scan rates ranging from 10 to 100 mV/s, as shown in Figure 5(C), and the calculated ECSA of MWCNTs@V_2O_5/Te differs from that of bare GCE. The values are obtained using the calibration plot shown in Figure 5(D). By using the Randles-Sevick equation [43];

$$ECSA = \frac{Cdl}{Cs} / 1000 \quad (5)$$

$$ECSA = 8.160 \times 10^{-4} / 2 \times 1000$$

$$ECSA = 0.000408 \times 1000$$

$$ECSA = 0.408\ cm^2$$

Here, Cdl and Cs represent the double-layer capacitance and specific capacitance, respectively. The ECSA of MWCNTs@V_2O_5/Te and bare GCE are 0.408 cm^2 and 0.073 cm^2, respectively [30, 49]. The prepared MWCNTs@V_2O_5/Te thus exhibits high supramolecular recognition capabilities and displays higher conductivity, resulting in an elevated surface area.

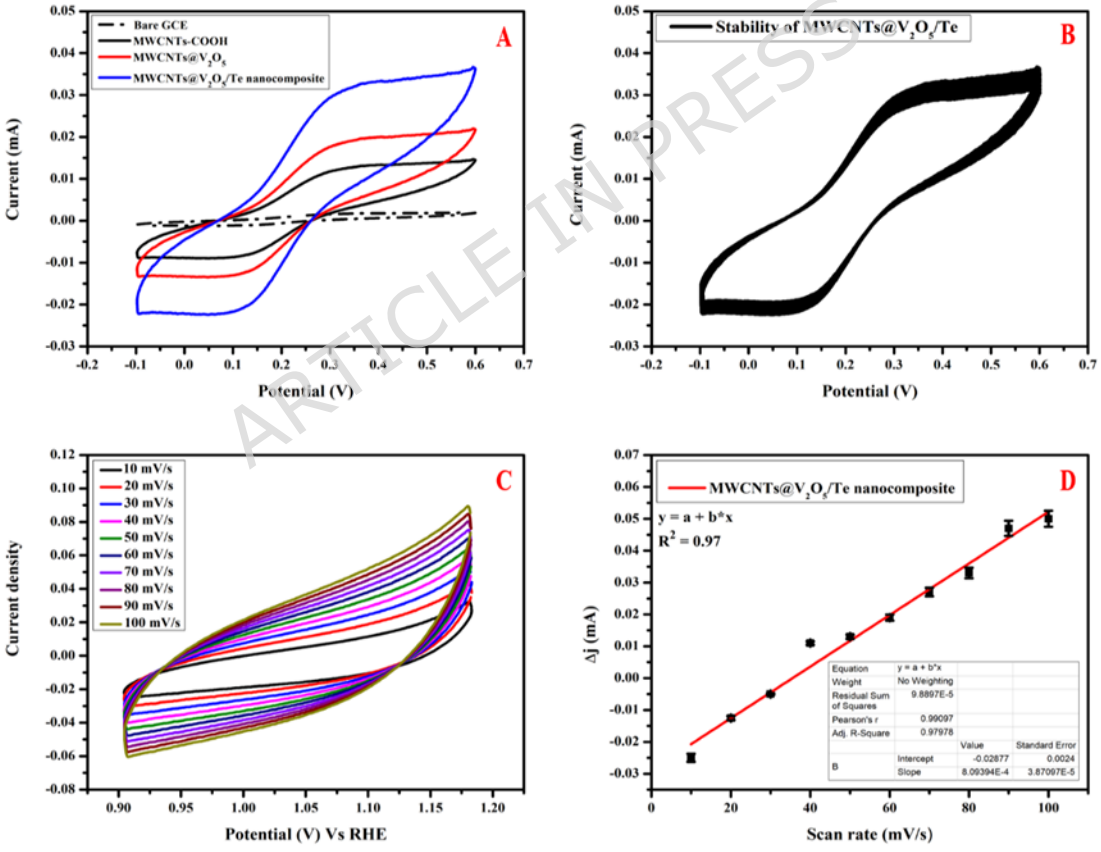

Figure 5. (A) Cyclic voltammograms (CV) indicate the electrical conductivities of bare GCE, MWCNTs- COOH, MWCNTs@V_2O_5, and MWCNTs@V_2O_5/Te. (B) Graph depicts stability of MWCNTs@V_2O_5/Te (C) ECSA curves of MWCNTs@V_2O_5/Te at varying scan rates, (D) Line graph of ECSA.

3.2.2 Roughness factor

The roughness factor (R_f) of the MWCNTs@V_2O_5/Te by GCE was usually determined by using the mentioned formula [43]:

$$R_f = \frac{A_2}{A_1} \quad (6)$$

where A_2 represents the ECSA of the MWCNTs@V_2O_5/Te electrode, i.e., 0.40, and A_1 represents the ECSA of the bare electrode, i.e., 0.073. The calculated Rf is approximately 5.4, providing valuable information about the texture and surface morphology of the MWCNTs@V_2O_5/Te electrode compared to the GCE. This higher Rf value indicates that the MWCNTs@V_2O_5/Te modification increased the electrochemically active surface area and the highly porous, rough electrode surface structure, providing a larger number of active sites for the electrochemical reaction.

3.2.3 Heterogeneous Electron Transfer Constant (k°)

The heterogeneous electron transfer constant (kº) is calculated using the following equation [43]:

$$k^\circ = \frac{RT}{F^2 R_{ct} A C} \quad (7)$$

where, the general gas constant (8.314 JK^{-1} mol^{-1}) is denoted by R, thermodynamic temperature (298.15 K) is denoted by T, Faraday's constant (96,485 C mol^{-1}) is denoted by F, C is the concentration of ($[Fe(CN)_6]^{3-/4-}$), R_{ct} is the electron transfer resistance i.e., 16640 Ω for bare GCE and 6286 Ω for MWCNTs@V_2O_5/Te and, A is the electrode surface

area. i.e., 0.073 cm^2 and 0.139 cm^2 for bare GCE and MWCNTs@V_2O_5/Te modified GCE, respectively. The electron-transfer constants for the bare GCE and the modified electrode MWCNTs@V_2O_5/Te are calculated using the formula given above. The k^0 for bare and modified GCE is 2.1 × 10^ (-6) cm/s, and 1.0 × 10^ (-6) cm/s, respectively. At the electrode surface, charge transfer is evaluated by electrochemical impedance spectroscopy **(**EIS). At various electrodes, the electrochemical impedance behavior is examined, and a reciprocal correlation is observed between electrical conductivity and surface resistance. The impedance study reveals that MWCNTs@V_2O_5/Te exhibits superior electron-transfer kinetics compared to bare GCE, attributed to its greater surface area.

3.3 Morphine Sulfate Detection in Drug Samples

3.3.1 Cyclic Voltammetry (CV)

An electrochemical technique, such as cyclic voltammetry (CS350M potentiostat/galvanostat with EIS), is used to measure the redox processes between the ligand and analyte [42]. In Figure 6(A), there is no oxidation-reduction activity on bare GCE. The oxidation peak current occurs at 0.4 V for analyte concentrations of 10 µM, 20 µM, 30 µM, 40 µM, 50 µM, and 60 µM. The maximum oxidation peak current is observed at 60 µM, and the minimum oxidation peak current is observed at 10 µM concentration. Whereas the reduction peak current occurs at -0.8 V in a 0.1 M PBS (pH 7.4) solution. There is a direct relationship between the concentration of morphine sulfate and the oxidation peak current, which means that as the morphine sulfate concentration increases, the peak current also increases, as shown in Figure 6(B), and its linearity (R^2) is around 0.98. Similarly, in Figure 6(C), the oxidation peak current occurs at 0.4 V across different pH values (6.6, 6.8, 7.0, 7.2, 7.4, and 7.8), indicating a varied effect. The result suggests that the maximum oxidation peak current occurs between the ligand and the analyte at pH 7.4, as it is the optimum pH. Whereas the minimum oxidation peak current is observed at pH 6.6, a reduction peak current also occurs at -0.5 V, as illustrated in Figure 6(D). Figure 6(E) shows a stability graph,

indicating that MWCNTs@V_2O_5/Te-Cys/GCE is highly stable for the determination of morphine sulfate.

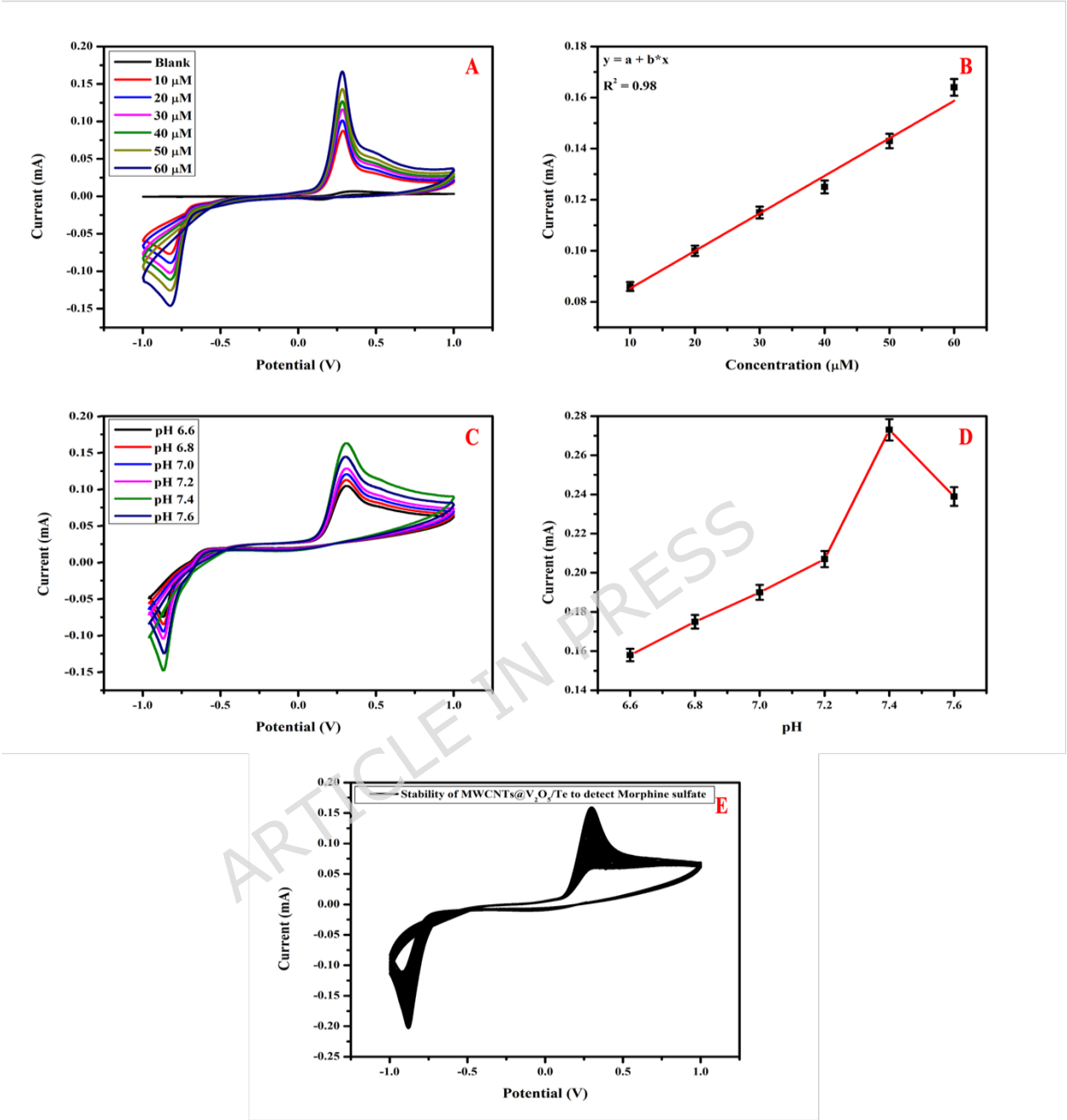

Figure 6. *Cyclic voltammetry (CV) (**A**) illustrates the effect of varying concentrations 10-60 µM of morphine sulfate, (**C**) the varying effect of pH 6.6-7.6 on the electrochemical behavior of biosensor for detection of morphine sulfate, (**B**) linear graph for analyte with varying concentrations, and (**D**) line graph with analyte at varying pH ranges, (**E**) stability of developed biosensor to detect morphine sulfate.*

3.3.2 Differential Pulse Voltametric (DPV) Analysis

Differential pulse voltammetry (DPV) measures differences in the rate of charging decay and Faradaic current when an amplitude-pulsed potential is applied [44]. In a blank solution of PBS (0.1 M), no oxidation-reduction reaction is observed. However, increasing the morphine sulphate concentration results in a gradual increase in the oxidation peak current. In Figure 7(A), the highest peak current is observed with 60 µM at 0.0mA current and 0.4 V potential, whereas the lowest peak is observed at 10 µM at 0.02 mA current and 0.4 V potential in a 0.1 M PBS solution of pH about 7.4. DPV follows the same trend as cyclic voltammetry, with a gradual increase in morphine sulfate concentration resulting in a rise in the oxidation peak current. In Figure 7(B), the calibration plot of concentration is shown, with a linearity (R^2) of around 0.99. Figure 7(C) examines the effect of pH, i.e., 6.6, 6.8, 7.0, 7.2, 7.4, and 7.6, on the determination phenomena. pH 7.4 yields the maximum peak current because it is the optimum pH at which the maximum number of oxidation reactions occur, whereas at pH 6.6, the minimum peak current is observed. Figure 7(D) illustrates the line graph. To summarize our results, we can confidently say that pH changes significantly influence the electrochemical activity of morphine sulfate.

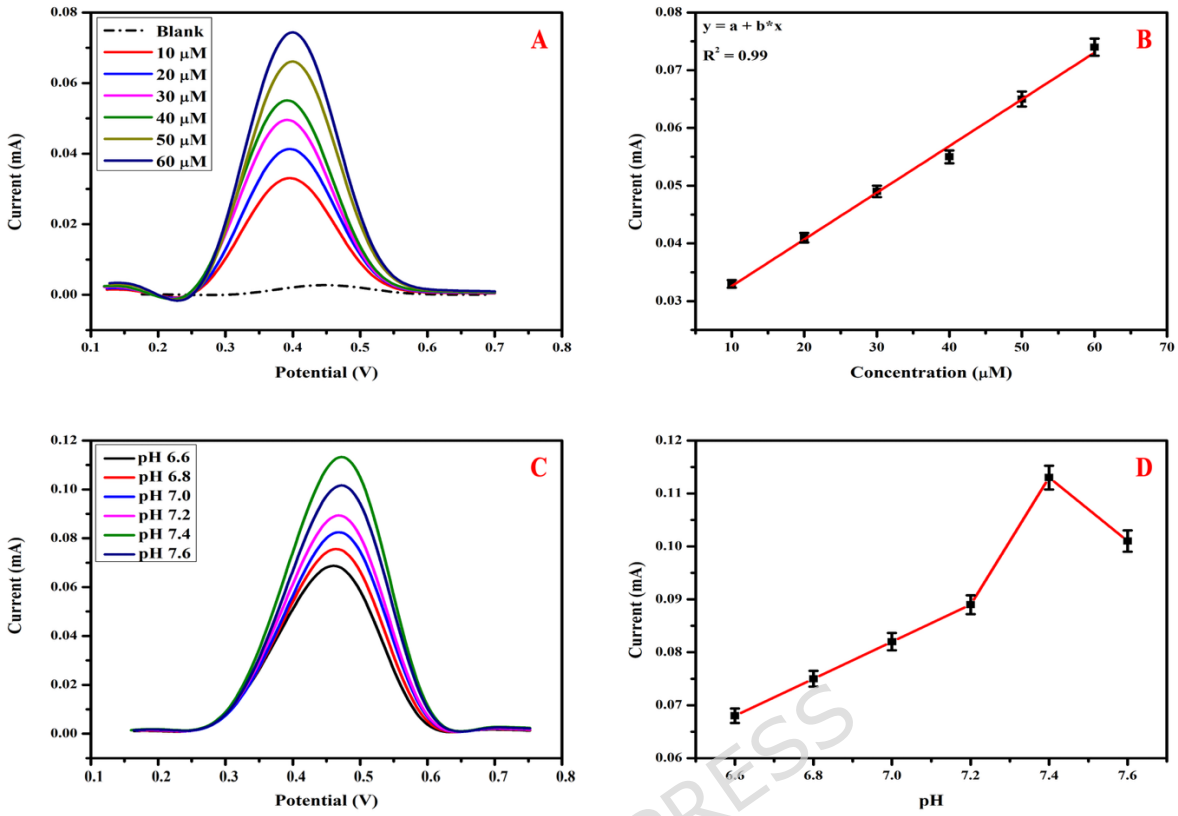

Figure 7. *Differential pulse voltammogram (DPV) (**A**) illustrates the effect of varying concentrations of 10-60 µM of morphine sulfate, (**B**) linear graph for analyte with varying concentrations, (**C**) the varying effect of pH 6.6-7.6 on the electrochemical behavior of biosensor for morphine sulfate detection, and (**D**) line graph for analyte at varying pH ranges.*

3.3.3 Mechanism of Electrochemical Sensing of Morphine Sulfate

At the electrode surface, the electrochemical sensing of morphine sulfate leads to an oxidation peak. As that MWCNTs@V_2O_5/Te nanocomposite was functionalized with the linker cysteamine (act as a linking agent) as cysteamine has -SH group which create thioether bond interaction with the -OH group of the MWCNTs@V_2O_5/Te nanocomposite and at the other end of the linker free -NH_2 group react with the -OH group on morphine sulfate in the presence of the iron as enzyme, employed in form of ferric cyanide is illustrated in Figure 8. Cysteamine, a short-chain linker, increases surface reactivity and selectivity towards morphine via thiol/amine interactions, which are structurally more favorable than

those of cystine for molecular orientation at the electrode surface. This cysteamine binding enables efficient capture and detection, enhancing the overall performance of the MWCNTs@V_2O_5/Te biosensor and facilitating the identification of morphine sulfate at low concentrations.

In electrochemical detection, the oxidation and reduction of morphine sulfate involve the electrode surface transitioning through several redox states. Electrochemical behavior of morphine sulfate is investigated by using CV, DPV, EIS, and chronoamperometry. Morphine sulfate undergoes oxidation at the anode; during this oxidation process, electrons from the morphine sulfate are lost. Typically, this results in the formation of a morphine sulfate radical cation or an oxidized product, which is subsequently reduced at the cathode. Electrons are gained during the reduction process, leading to the regeneration of morphine sulfate or a reduced form. The electrochemical response exhibits distinctive current peaks resulting from oxidation and reduction processes, and the peak heights vary with the amount of morphine sulfate in the sample. Based on the current response noted during electrochemical measurements, electrochemical sensors utilize these redox processes to identify and monitor morphine sulfate levels.

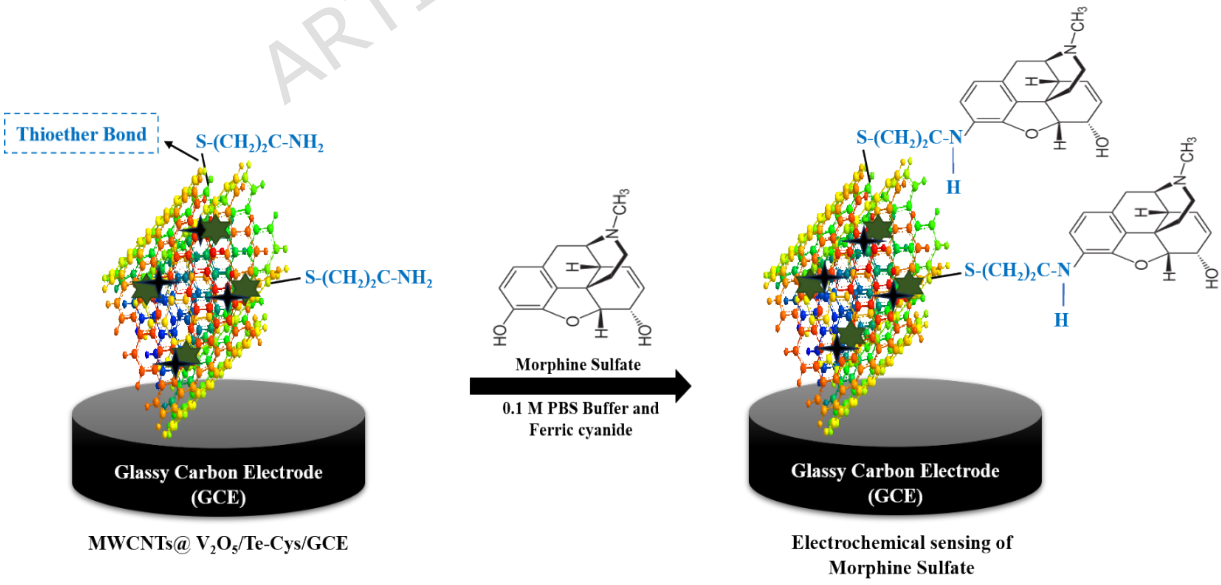

Figure 8. *Represent the mechanism of morphine sulfate sensing by MWCNTs@V_2O_5/Te-Cys/GCE.*

3.3.4 Limit of Detection (LOD) evaluation

LOD evaluation was performed to detect the lowest or least detectable quantity of morphine sulfate using MWCNTs@V_2O_5/Te/GCE. LOD is influenced by a variety of factors, including the buffer condition and matrix. With the help of the following formula, LOD is determined:

$$\text{LOD} = 3\frac{s}{m} \quad (8)$$

In this equation, standard deviation is denoted by s, while m represents the slope. For DPV, the calculated LOD is approximately 0.01 µM.

3.3.5 Reproducibility

This newly developed electrochemical sensor exhibits remarkable reproducibility in detecting morphine sulfate in PBS solution at various current, potential, scan rate, and temperature conditions. It is depicted in Fig. S1 (supporting information) upon examination by CV and DPV. As a result, this electrochemical sensor can be commercialized for various clinical diagnoses and laboratory applications.

3.3.6 Electrochemical Impedance Spectroscopy (EIS) Analysis

Resistance to charge transfer is evaluated using Electrochemical Impedance Spectroscopy (EIS) at various morphine sulfate concentrations and pH levels. Additionally, EIS analysis facilitates the evaluation of electrode response and electrode modifications. With an Rct probe, kinetics are studied at the electrode surface. To analyze the parameter R_{ct}, in the presence of the redox probe, Ag/AgCl/ 3M KCl, plot Nyquist curves. EIS is typically performed in solution using a 1:1 M ratio of KCl (0.1 M) and $[Fe(CN)_6]^{3-/4-}$ (0.1 mM). Using the Randles equivalent circuit, a Nyquist plot was fitted, and the Rct value can be obtained, indicating that quantitative data can be obtained from EIS. EIS is performed on both the bare electrode and the nanocomposite-modified electrode, yielding the Rct value.

Figure 9(A) illustrates that the R_{ct} value for the modified MWCNTs@V_2O_5/Te/GCE is 6286 Ω, which is smaller than the R_{ct} value for the bare GCE, i.e., 16640 Ω. This value indicates that electron transfer between the surface of the modified (MWCNTs@V_2O_5/Te) electrode and the morphine sulfate solution is faster, primarily due to the conductive nature of MWCNTs@V_2O_5/Te on the GCE. Additionally, there is minimal resistance to charge transfer between the modified electrode and morphine sulfate, indicating improved sensing abilities. EIS is measured using MWCNTs@V_2O_5/Te-Cys/GCE in different concentrations of morphine sulfate. Figure 9(B) illustrates that at a higher concentration of 60 µM of morphine sulfate, there is faster and maximum electron transfer between the morphine sulfate and the MWCNTs@V_2O_5/Te, as well as lower resistance in charge transfer on the surface of the MWCNTs@V_2O_5/Te/GCE, which is affected by the electrostatic interaction between the morphine sulfate and the developed electrochemical sensor. Regarding impedance, the effects of pH on morphine sulfate solutions are attributed to charge-transfer processes. The impedance graph at pH values ranging from 6.6 to 7.6 is shown in Figure 9(C), indicating that maximum electron transfer and minimum

resistance are observed at pH 7.4, which is the physiological optimum and ideal for enhanced electron transfer with reduced charge resistance.

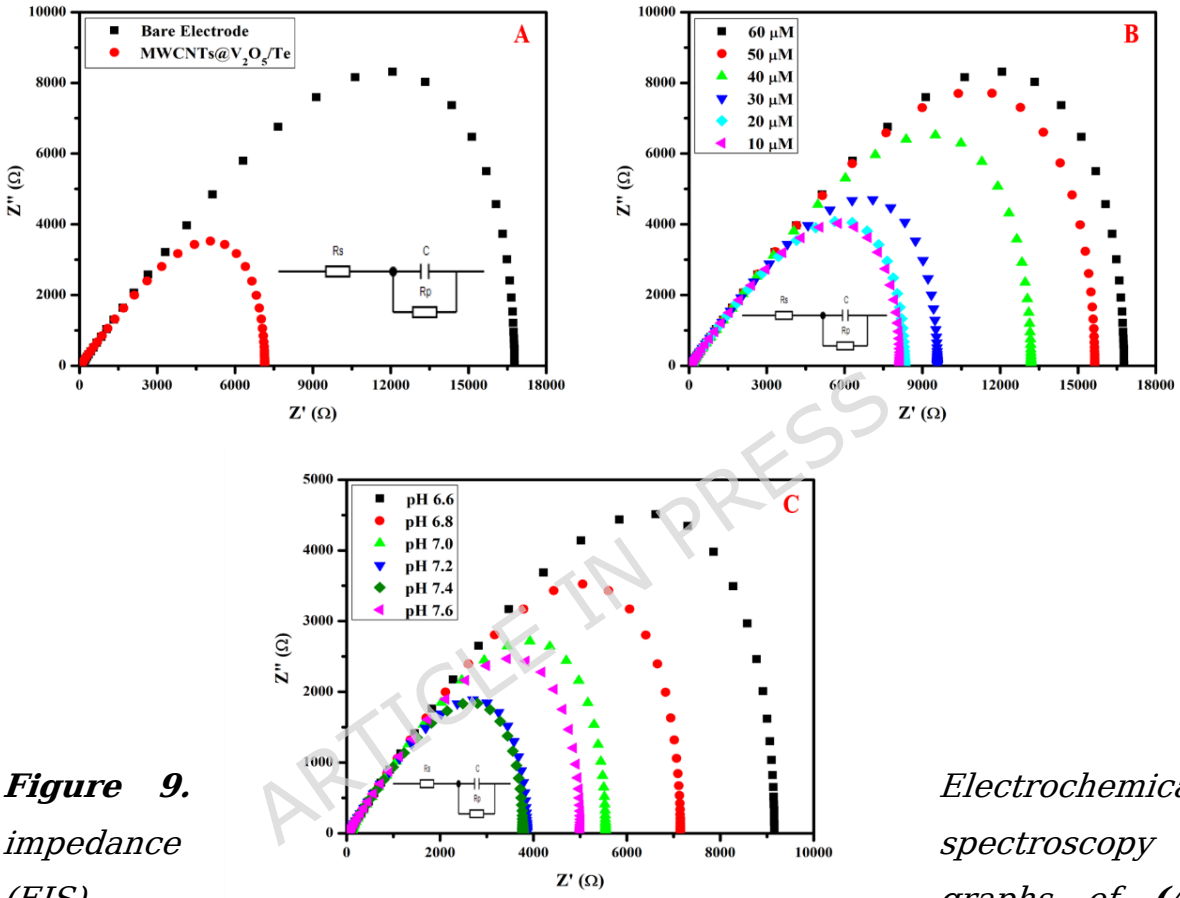

Figure 9. *Electrochemical impedance spectroscopy (EIS) graphs of* ***(A)*** *bare GCE and MWCNTs@V_2O_5/Te/GCE,* ***(B)*** *effect of varying morphine sulfate concentrations 10-60 µM,* ***(C)*** *the varying effect of pH 6.6-7.6 on the electrochemical response of the biosensor for morphine sulfate detection.*

3.3.7 Exponential factor

With the help of the following equation, the exponential factor is calculated:

$$\text{Exponential factor} = \frac{RT}{R^2 + (2\pi i f \times \tau)^2} \quad (9)$$

In this equation, charge transfer resistance is denoted by R, π is the circle's perimeter (~3.14), the frequency of the sinusoidal perturbation signal is denoted by f (i.e., 0.01 Hz), and τ is the time constant (i.e., τ = R × C), where C is the capacitance. The exponential factor for MWCNTs@V_2O_5/Te/GCE is 1.5 × 10^8, and for bare GCE, the value is 5.9 × 10^7 (R_{ct} for modified and bare GCE are 6286 and 16640 Ω). The exponential factors for detecting morphine sulfate at its optimum pH and concentration (Rct values of 3779 and 18146 Ω, respectively) are 2.1 × 10^8 and 5.4 × 10^^{7}, respectively.

3.4 Morphine Sulfate Detection in Serum Samples

Morphine reaches its half-life in 3-4 hours, at which point its concentration in the rabbit's body is reduced by 50%. The fabricated biosensor demonstrated outstanding potential for determining morphine levels at different times in the serum sample. After morphine administration, blood samples were taken at various time intervals (i.e., 2, 4, and 6 h) and analyzed via CV and DPV, as shown in Fig. 10. For comparison, serum samples were extracted when morphine was not administered and labeled as the control. The sensor showed no response when the control sample was run. A sharp peak is observed during the first 1-3 hours, indicating the drug's maximum serum concentration. As time passes, the current intensity decreases, indicating the elimination of morphine sulfate from the rabbits' biofluids. A slight variation in current levels is observed, suggesting that other factors, such as metabolic rates, contribute to the differences. With the help of the following formula, LOD is determined:

$$\mathrm{LOD} = 3\frac{s}{m} \quad (10)$$

In this equation, standard deviation is denoted by s, while m represents the slope. For CV and DPV, the calculated LODs in serum samples are about 0.03 µM and 0.02 µM, respectively.

Recently employed biosensors, their sensing parameters, linear ranges, and LODs for detecting morphine sulfate in real biological samples are shown in **Table 1**. MWCNTs@V_2O_5/Te-Cys is employed to detect morphine sulfate. MWCNTs have increased the conductivity and surface area of this nanocomposite, while the redox-active V_2O_5 nanorods promote charge transfer between the nanocomposite and morphine sulfate. Cysteamine further increases surface reactivity and selectivity toward morphine via thiol/amine interactions. The MWCNTs@V_2O_5/Te-Cys biosensor has improved conductivity, specificity, selectivity, and reproducibility compared to previous biosensors. Lower detection limits are another unique attribute of this biosensor, making it more effective for detecting trace analytes.

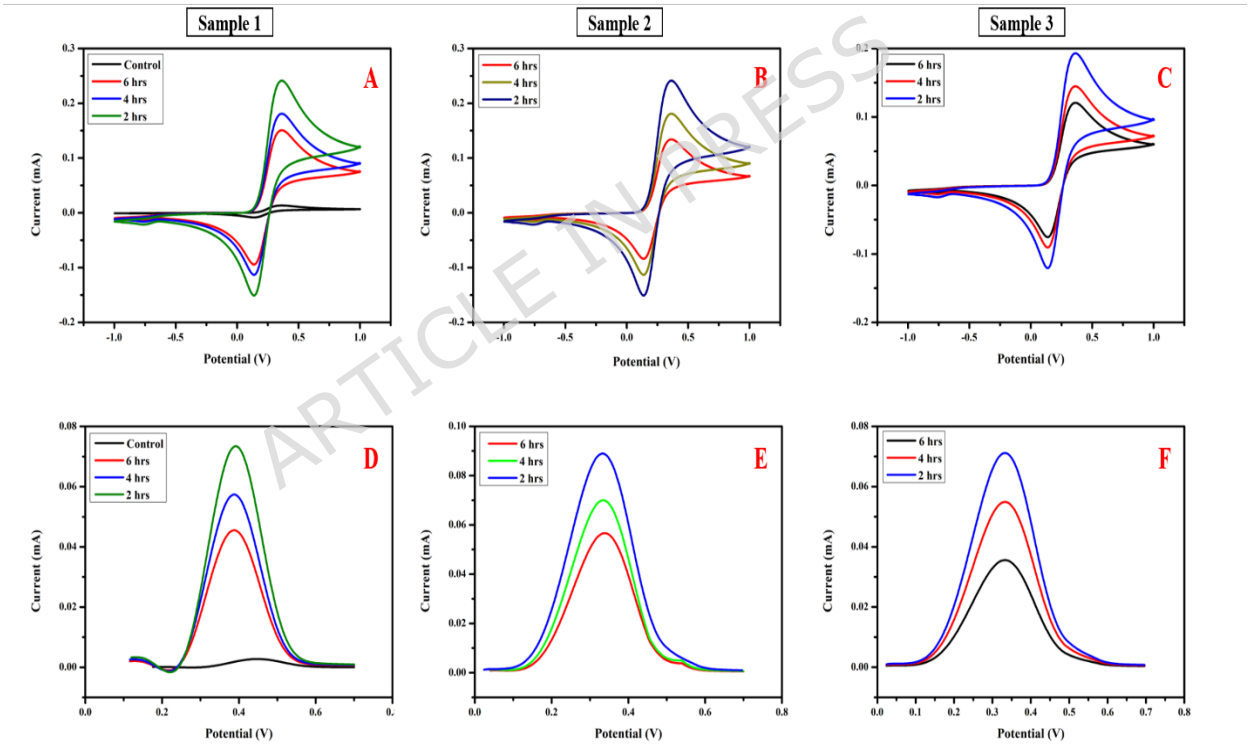

Figure 10. *MWCNTs@V_2O_5/Te-Cys/GCE used for the detection of morphine sulfate in real biological samples at different time intervals via* ***(A-C)*** *cyclic voltammetry (CV),* ***(D-F)*** *differential pulse voltammetry (DPV).*

Table 1. *Recently employed biosensors, their sensing parameters, linear ranges, and LODs for detecting morphine sulfate in real biological samples.*

Sr. no	Electrochemical sensors	Sensing parameters	Linear range	LOD	Ref
1.	CdSe-doped Graphene oxide	CV, DPV	0.1-20 µM	0.03 µM	[45]
2.	TGA-CdSe/ZnS@FCNT	DPV, CV	0.08-100 µM	0.024 µM	[46]
3.	Au NDs/BHCS	CV, DPV	0.01-300 µM	8.3 nM	[47]
4.	MgO/SWCNTs/MOCITFB/ CPE	CV	3.0-320 µM	0.8 nM	[48]
5.	$FeWO_4$/CPE	SWV	5-85 µM	0.58 µM	[1]
6.	Poly(CTAB)/GO/GCE	CV	50-60 µM	0.36 µM	[49]
7.	β-MnO2-NF/GCE	DPV, CV	0.1-200 µM	8.3 nM	[50]
8.	Graphene oxide/MWCNTs/ zinc oxide nanorods/ polypyrrole	CV	0.04-100 µM	0.01 µM	[51]
9.	Gd2Te3@Sm-Cystine/GCE	CV, LSV, and DPV	20-60 µM	1.29, 3.9 µM	[52]
10.	MWCNTs@V_2O_5/Te-Cys/GCE	CV, DPV, and EIS	10-60 µM	0.01 µM	**Current work**

3.5 Recovery Analysis of morphine sulfate by MWCNTs@V_2O_5/Te

Recovery analysis for morphine sulfate in serum samples is measured by MWCNTs@V_2O_5/Te-Cys/GCE. Serum samples are diluted 10-fold in 7.4 pH PBS buffer. Table S1 shows recovery rates ranging from 85% to 98%, indicating the potential applicability of MWCNTs@V_2O_5/Te-Cys for detecting morphine sulfate in serum samples and the accuracy of the fabricated methodology.

3.6 Chronoamperometric Analysis

Chronoamperometry is used to evaluate the durability, steady-state activity, and stability of the designed electrochemical biosensor. A chronoamperometric curve of MWCNTs@V_2O_5/Te with cysteamine is obtained at a scan rate of approximately 50 mV/s for 14 hours. Figure 11 (A) depicts the linear response. Within the first two hours, the current decreases sharply; thereafter, it remains constant, indicating the consistency and stability of the designed electrochemical biosensor. An interference study checks the stability and selectivity of the designed electrochemical sensor towards morphine sulfate. The interfering species employed included paracetamol, albumin, hemoglobin, glucose, and sucrose in the morphine-PBS solution at 60 µM, as illustrated in Figure 11(B). Due to interference from other species, the results indicate a minor decrease in the biosensor's current response to the analyte.

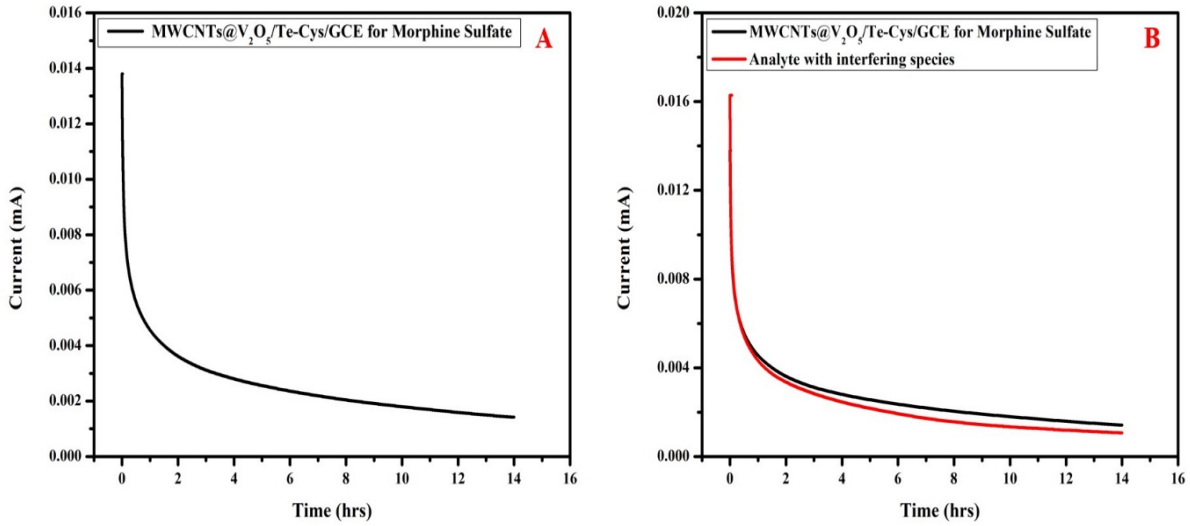

Figure 11. (A) *Chronoamperometric graph of* GCE, ***(B)*** *Chronoamperometric graph in the presence of interfering species.*

3.6.1 Amperometric Selectivity Coefficient

The designed electrochemical biosensor's amperometric selectivity coefficient is calculated with the help of the following equation:

$$i_t = K\,(C_i + \sum k_{ij}^{amp}\, C_j) \quad (11)$$

In this equation, the value of K was ≤≤1 (i.e., the catalytic reaction rate constant), the concentration of the morphine sulfate (target analyte) is represented by C_i, which is 10 µM, the concentration of the interfering species is represented by C_j, which is also 10 µM, and the total current is indicated by i_t. The amperometric selectivity coefficient is represented by $\sum k_{ij}^{amp}$. For the detection of the target analyte, a higher value of ∑kijamp suggests that, during amperometric measurement, other species will interfere with the sensing capability of the developed electrochemical biosensor. The calculated amperometric selectivity coefficient ($\sum k_{ij}^{amp}$) for morphine sulfate detection was approximately 1.5×10^{-11}, indicating that the developed immunosensor is highly stable and can be used in the near future for further clinical diagnosis and for the detection of a variety of analytes.

Conclusion

In this work, a novel detection and quantification method for morphine sulfate in real biological samples is developed for the first time using a MWCNTs@V_2O_5-Te/GCE biosensor, offering high reproducibility. This electrochemical method offers on-site, real-time analysis and ease of handling. This synthesized biosensor enhanced the surface area and conductivity of bare GCE. The structural results reveal that MWCNTs@V_2O_5/Te-Cys is successfully synthesized and exhibits favorable electrochemical behavior for the detection of morphine sulfate in serum samples, as analyzed by CV, DPV, and EIS at various concentrations and pH values. Chronoamperometry measures the stability of the modified electrode, eliminating interference from other species. The developed electrochemical sensor exhibited high stability and selectivity, with exceptional bioanalytical performance for the determination of morphine sulfate in pharmaceutical analysis and in real biological samples. The fabricated detection method can contribute to the development of efficient and reliable analytical techniques for studying narcotics, forensic analysis, clinical diagnosis, and drug delivery systems. It will revolutionize point-of-care (POC) devices.

Acknowledgement

The authors acknowledge the Higher Education Commission (HEC) of Pakistan for the financial support (20-16797/NRPU/R&D/HEC/2021) for this work.

Declaration

Conflict of Interest

Authors declare no financial or competing interests in this study.

Ethical Approval

Ethical approval for sample collection and analysis was obtained from the Ethics Committee of Bahauddin Zakariya University, Multan, Pakistan.

Data Availability Statement

All the data is provided in the manuscript and supporting information.

Funding

This reseaech was supported by Higher Education Commission (HEC) of Pakistan through National Research Program for Universities (20-16797/NRPU/R&D/HEC/2021).

References

1. Ognjanović, M., et al., *Electrochemical Determination of Morphine in Urine Samples by Tailoring FeWO4/CPE Sensor.* Biosensors, 2022. **12**(11): p. 932.
2. Salavert, A., et al., *Direct dating reveals the early history of opium poppy in western Europe.* Scientific reports, 2020. **10**(1): p. 20263.
3. Hayat, M.T., U. Hameed, and M. Zia-Ul-Haq, *Opium Poppy*, in *Essentials of Medicinal and Aromatic Crops*. 2023, Springer. p. 935-964.
4. Tavlı, Ö.F., *Papaver somniferum L*, in *Novel Drug Targets With Traditional Herbal Medicines: Scientific and Clinical Evidence*. 2022, Springer. p. 479-494.
5. Vadhel, A., et al., *Opium alkaloids, biosynthesis, pharmacology and association with cancer occurrence.* Open Biology, 2023. **13**(5): p. 220355.
6. Nosek, K., et al., *Efficacy and safety of topical morphine: a narrative review.* Pharmaceutics, 2022. **14**(7): p. 1499.
7. Noufal, Y., et al., *Pharmacological data science perspective on fatal incidents of morphine treatment.* Pharmacology & Therapeutics, 2023. **241**: p. 108312.
8. Zarin, M.K.Z., et al., *Synthesis and Modification of Morphine and Codeine, Leading to Diverse Libraries with Improved Pain Relief Properties.* Pharmaceutics, 2023. **15**(6): p. 1779.
9. Badshah, I., et al., *Molecular mechanisms of morphine tolerance and dependence; novel insights and future perspectives.* Molecular and Cellular Biochemistry, 2023: p. 1-29.
10. Murphy, P.B., S. Bechmann, and M.J. Barrett, *Morphine*. 2023, StatPearls Publishing, Treasure Island (FL).
11. Yasien, S., et al., *Simultaneous quantification of opioids in blood and urine by gas chromatography-mass spectrometer with modified dispersive solid-phase extraction technique.* Molecules, 2022. **27**(19): p. 6761.
12. Jain, R., et al., *A rapid and cost-effective method based on dispersive liquid -liquid microextraction coupled to injection port silylation-gas chromatography-mass spectrometry for determination of morphine in illicit opium.* Analytical Science Advances, 2021. **2**(7-8): p. 387-396.

13. Ghorani-Azam, A., et al., *Plant extract and herbal products as potential source of sorbent for analytical purpose: An experimental study of morphine and codeine determination using HPLC and LC–MSMS.* Journal of Chromatographic Science, 2021. **59**(5): p. 482-489.
14. Buratti, E., et al., *Validation of an HPLC-HR/MS method for the determination and quantification of six drugs (morphine, codeine, methadone, alprazolam, clonazepam and quetiapine) in nails.* Journal of Analytical Toxicology, 2023: p. bkad022.
15. Chow, K.L., et al., *Morphine-specific IgE testing in the assessment of neuromuscular blocking agent allergy: a single centre experience.* British journal of anaesthesia, 2023.
16. Zarad, W., et al., *Field amplified sample stacking and in-capillary derivatization for forensic analysis of morphine and morphine-6-glucuronide in human urine by capillary electrophoresis.* Talanta Open, 2021. **3**: p. 100041.
17. Jahani, P.M., et al., *Electrochemical sensor for acetylcholine detection based on WO3 nanorods-modified glassy carbon electrode.* Journal of Electrochemical Science and Engineering, 2024. **14**(5): p. 631-641.
18. Azizpour Moallem, Q. and H. Beitollahi, *Modified Carbon Paste Electrode based on Cu-BTC MOF: Electrochemical Detection of Epinephrine in the Presence of Acetaminophen.* Journal of Environmental and Bioanalytical Electrochemistry, 2025. **1**(1): p. 1-14.
19. Tajik, S., et al., *Two-dimensional Co-based metal-organic framework nanosheets as an efficient electrochemical sensing platform for simultaneous determination of daunorubicin and idarubicin.* ADMET and DMPK, 2025. **13**(2).
20. Tajik, S., R. Moghimian, and H. Beitollahi, *Epirubicin-sensitive detection with a CoWO4/reduced graphene oxide modified screen-printed electrode.* ADMET and DMPK, 2025. **13**(3).
21. Tajik, S., et al., *Electrochemical sensor based on multi-walled carbon nanotubes and two-dimensional zeolitic imidazolate framework nanosheets: Application in determining dacarbazine.* ADMET and DMPK, 2025. **13**(1).
22. Knežević, S., et al., *La (OH) 3 Multi-Walled Carbon Nanotube/Carbon Paste-Based Sensing Approach for the Detection of Uric Acid—A Product of Environmentally Stressed Cells.* Biosensors, 2022. **12**(9): p. 705.
23. Knežević, S., et al., *Sensing Platform Based on Carbon Paste Electrode Modified with Bismuth Oxide Nanoparticles and SWCNT for Submicromolar Quantification of Honokiol.* Food Analytical Methods, 2022: p. 1-12.
24. Stanković, D.M., et al., *CeO2-doped–domestic carbon material decorated with MWCNT as an efficient green sensing platform for electrooxidation of dopamine.* Surfaces and Interfaces, 2021. **25**: p. 101211.
25. Malhotra, B.D. and M.A. Ali, *Nanomaterials in biosensors: Fundamentals and applications.* Nanomaterials for biosensors, 2018: p. 1.
26. Cho, I.-H., et al., *Current technologies of electrochemical immunosensors: Perspective on signal amplification.* Sensors, 2018. **18**(1): p. 207.
27. Holzinger, M., A. Le Goff, and S. Cosnier, *Nanomaterials for biosensing applications: a review.* Frontiers in chemistry, 2014. **2**: p. 63.
28. Shaheen, S., et al., *Immobilization of antivenom polyvalent antibodies on MWCNTs@ WO3-Co3O4 capped with 3-mercaptopropionic acid for developing impedimetric immunosensor for snake venom detection.* Microchemical Journal, 2025. **209**: p. 112797.

29. Tan, S., et al., *Conductive coating, cation-intercalation, and oxygen vacancies co-modified vanadium oxides as high-rate and stable cathodes for aqueous zinc-ion batteries.* EcoMat, 2023. **5**(4): p. e12326.
30. Gamal, H., et al., *Recent advances of vanadium oxides and their derivatives in supercapacitor applications: A comprehensive review.* Journal of Energy Storage, 2024. **76**: p. 109788.
31. Han, M., et al., *Highly conductive tellurium and telluride in energy storage.* ChemElectroChem, 2021. **8**(23): p. 4412-4426.
32. Padmanaban, A., et al., *Hexagonal phase Pt-doped cobalt telluride magnetic semiconductor nanoflakes for electrochemical sensing of dopamine.* Journal of Electroanalytical Chemistry, 2020. **877**: p. 114658.
33. Seo, Y., et al., *Synthesis of multi-walled carbon nanotubes modified with silver nanoparticles and evaluation of their antibacterial activities and cytotoxic properties.* JoVE (Journal of Visualized Experiments), 2018(135): p. e57384.
34. Sun, H., et al., *Zinc oxide/vanadium pentoxide heterostructures with enhanced day-night antibacterial activities.* Journal of colloid and interface science, 2019. **547**: p. 40-49.
35. Zhou, X., et al., *The synthesis, characterization and electrochemical properties of Multi-Wall Carbon Nanotube-induced vanadium oxide nanosheet composite as a novel cathode material for lithium ion batteries.* Electrochimica Acta, 2012. **74**: p. 32-38.
36. Park, D., H. Ju, and J. Kim, *Preparation and thermoelectric properties of two types of nanostructured tellurium with multi-walled carbon nanotubes.* Journal of Alloys and Compounds, 2018. **748**: p. 305-313.
37. Eissa, S. and M. Zourob, *Competitive voltammetric morphine immunosensor using a gold nanoparticle decorated graphene electrode.* Microchimica Acta, 2017. **184**: p. 2281-2289.
38. Haniyeh, F., A. Abdollah, and D. Abolghasem, *Controlled growth of well-Aligned carbon nanotubes, electrochemical modification and electrodeposition of multiple shapes of gold nanostructures.* Materials Sciences and Applications, 2013. **2013**.
39. Gupta, V. and T.A. Saleh, *Syntheses of carbon nanotube-metal oxides composites: adsorption and photo-degradation.* Carbon Nanotubes-From Research to Applications, 2011. **17**: p. 295-312.
40. Sahuaro, H., *Obtaining nano structures of cobalt telluride by a simplified ion exchange reaction at aqueous solution.* Chalcogenide Letters, 2019. **16**(2): p. 57-61.
41. Alghool, S., H.F. Abd El-Halim, and A.M. Mostafa, *An eco-friendly synthesis of V 2 O 5 nanoparticles and their catalytic activity for the degradation of 4-nitrophrnol.* Journal of Inorganic and Organometallic Polymers and Materials, 2019. **29**: p. 1324-1330.
42. Elgrishi, N., et al., *A practical beginner's guide to cyclic voltammetry.* Journal of chemical education, 2018. **95**(2): p. 197-206.
43. Fatima, B., et al., *Facile hydrothermal synthesis of NiTe nanorods for non-enzymatic electrochemical sensing of whole blood hemoglobin in pregnant anemic women.* Analytica Chimica Acta, 2022. **1189**: p. 339204.
44. Budiyanto, F. and A. Bayu, *Bioelectrochemical systems for managing the metal's issues*, in *Bioremediation, Nutrients, and Other Valuable Product Recovery*. 2021, Elsevier. p. 41-82.
45. Nazari, Z. and Z. Es' haghi, *A new electrochemical sensor for the simultaneous detection of morphine and methadone based on thioglycolic acid decorated CdSe doped graphene oxide multilayers.* Analytical and Bioanalytical Electrochemistry, 2022. **14**(2): p. 228-245.

46. Nazari, Z. and Z. Eshaghi, *Carbon Nanotube Reinforced Heterostructure Electrochemical Sensor for the Simultaneous Determination of Morphine and Fentanyl in Biological Samples.* Iranian Journal of Analytical Chemistry, 2022. **9**(1): p. 63-77.
47. Imanzadeh, H., et al., *Broken hollow carbon spheres decorated by gold nanodendrites as the advanced electrochemical sensing platform for sensitive tracing of morphine in human serum and saliva.* Sensors and Actuators B: Chemical, 2024. **398**: p. 134738.
48. Zare, S.J., et al., *Amplified electrochemical sensor for nano-molar detection of morphine in drug samples.* Int. J. Electrochem. Sci, 2021. **16**(1).
49. Abraham, P., et al., *Electrochemical synthesis of thin-layered graphene oxide-poly (CTAB) composite for detection of morphine.* Journal of Applied Electrochemistry, 2020. **50**: p. 41-50.
50. Akbari, S., et al., *Simultaneous determination of methadone and morphine at a modified electrode with 3D β-MnO 2 nanoflowers: application for pharmaceutical sample analysis.* RSC advances, 2020. **10**(63): p. 38532-38545.
51. Nazari, Z., Z. Es' haghi, and H. Liu, *Improving Electrochemical Performance of Polypyrrole Coating by Graphene Oxide-Carbon Nanotube and Zinc Oxide Nanorods in the Role of a Sensor for the Simultaneous Measurement of Morphine and Methadone.* Analytical and Bioanalytical Chemistry Research, 2023. **10**(2): p. 205-225.
52. Subhan, M., et al., *Highly sensitive detection of opium alkaloid morphine sulfate in blood sample using cystine modified samarium doped gadolinium telluride biosensor.* Microchemical Journal, 2025: p. 114307.